PENNSTATE

Applied Research Laboratory

# Low-Wavenumber Wall Pressure Fluctuations due to Boundary - Layer Transition

G.C. Lauchle and S. Park

Technical Memorandum
File No. 00-100
18 May 2000

Copy No. 45

**DISTRIBUTION STATEMENT A**
**Approved for Public Release**
**Distribution Unlimited**

Applied Research Laboratory
P.O. Box 30
State College, PA 16804

# Low-Wavenumber Wall Pressure Fluctuations due to Boundary-Layer Transition

**G. C. Lauchle, S. Park**

Technical Memorandum
File No. 00-100
18 May 2000

**Never issued as IM**

Abstract: Boundary layer transition is an important contributor to sensor flow-induced self noise. The pressure fluctuations caused by this spatially bounded, and intermittent, phenomenon encompass a very wide range of spatial wavenumbers and temporal frequencies. Here, we analyze the wavevector-frequency spectrum of the wall pressure fluctuations due to subsonic boundary-layer transition as it occurs on a flat plate under zero pressure gradient conditions. Based on previous measurements of the statistics of the boundary-layer intermittency, it is found that transition induces higher low-streamwise wavenumber wall pressure levels than does a fully-developed turbulent boundary layer (TBL) that might superficially exist at the same location and at the same Reynolds number. The transition zone spanwise wavenumber pressure components are virtually unchanged from the TBL case. The results suggest that transition may be more effective than the TBL in forcing structural excitation at low Mach numbers, and it may have a more intense radiated noise contribution on a per unit area basis. This may help explain increases in measured sensor self noise when the sensors are placed near the transition zone.

Acknowledgment: This work was supported by the ONR, Code 333, Grant No. N00014-99-1-0259. This report represents the **Final Report** for this grant.

# TABLE OF CONTENTS

## LIST OF FIGURES

## INTRODUCTION

Acoustic sensors that are placed flush to the surface of a vehicle are typically used to measure acoustic energy originating from some distant source, such as in sonar applications. If those sensors are placed under the turbulent boundary layer (TBL) of the vehicle, formed because the vehicle is moving through the medium at some mean speed, $U_\infty$, then the effectiveness of the sensors in hearing the acoustic signals of interest is seriously diminished due to flow-induced sensor self noise. This self noise depends strongly on the speed of the vehicle, on whether the TBL is developing in a zero, favorable, or adverse static pressure gradient, and on the proximity of the sensors relative to the beginning and ends of the TBL. If placed near the end of the TBL, the resulting sensor self noise will have significant *additional* contributions due to trailing edge noise mechanisms including local flow separation. If the sensors are situated near the beginning of turbulent flow, the laminar-to-turbulent transition zone noise mechanisms contribute. The wall pressure fluctuations generated by TBL's, transition zones, separated flows, and edge flows are stochastic fields that have spectral characteristics rich in both frequency and wavenumber content. Wall pressure fluctuations can couple efficiently to the structural modes of the vehicle supporting these flows if the structural modal frequencies and flexural wavenumbers correspond to those of the pressure fluctuations. This adds additional energy to the sensor self noise spectrum, and also to the radiated noise levels of the vehicle as a whole.

For underseas applications, where the structures are thick and massive, and the mean flow Mach numbers are very low, this coupling occurs predominantly in the so-called *low-wavenumber regime*. At a particular radian frequency, say $\omega'$, the majority of the turbulent spectral energy occurs near the convective wavenumber, $k_c \sim \omega'/u_c$, where $u_c$ is the convection speed of turbulent eddies in the boundary layer, typically $\sim 0.7U_\infty$. The acoustic radiation from the turbulence occurs only at sonic and supersonic wavenumbers, $k \leq k_o$, where $k_o = \omega'/c_o$ with $c_o$ being the sound speed. Clearly, $k_o/k_c \sim M_c$, the convective Mach number. In underwater situations, say $U_\infty \sim 15$ m/s, $M_c \sim 10^{-2}$. Two orders of magnitude spans these two important wavenumbers; this is the low-wavenumber regime. Now if $\omega'$ corresponds to a resonant frequency of the vehicle skin, and the wavelength of the corresponding flexural mode is $\lambda_p$, then the structural wavenumber at this frequency is $2\pi/\lambda_p$. These wavenumbers invariably reside in the low-wavenumber regime, and it is for this and related reasons, why considerable contemporary research has focused on understanding the low-wavenumber wall pressure fluctuations induced by TBL's and related flows. The reader is referred to the books by Howe[1] and Blake[2] for a complete treatment of the issues for zero-pressure gradient TBL's, separated, and edge flows. Farabee[3] provides additional comprehensive information on the wall pressure statistics associated with non-equilibrium TBL's, while Lauchle[4] reviews the hydroacoustics of boundary-layer transition.

The objective of the work described in this paper is to analyze the wavenumber-frequency characteristics of the wall pressure fluctuations induced by the laminar-to-turbulent transition region on a flat surface under zero pressure gradient, and very low, subsonic Mach number conditions. We are particularly interested in the low-wavenumber wall pressure components generated by transition, and how they compare to those of the TBL. This analysis provides new information that supports the notion that transition is an important source of both radiated and self noise for non-rigid vehicles supporting transition in the forward nose region.

## I. THE TRANSITION PROCESS

The *transition* of a laminar boundary layer into a turbulent one is characterized by the breakdown of hairpin vortices into spots of turbulence that are formed randomly in space and time. The spots grow as they convect, and they eventually coalesce to form the turbulent boundary layer. Figure 1 shows a flow visualization of this process for an axisymmetric body.[5]

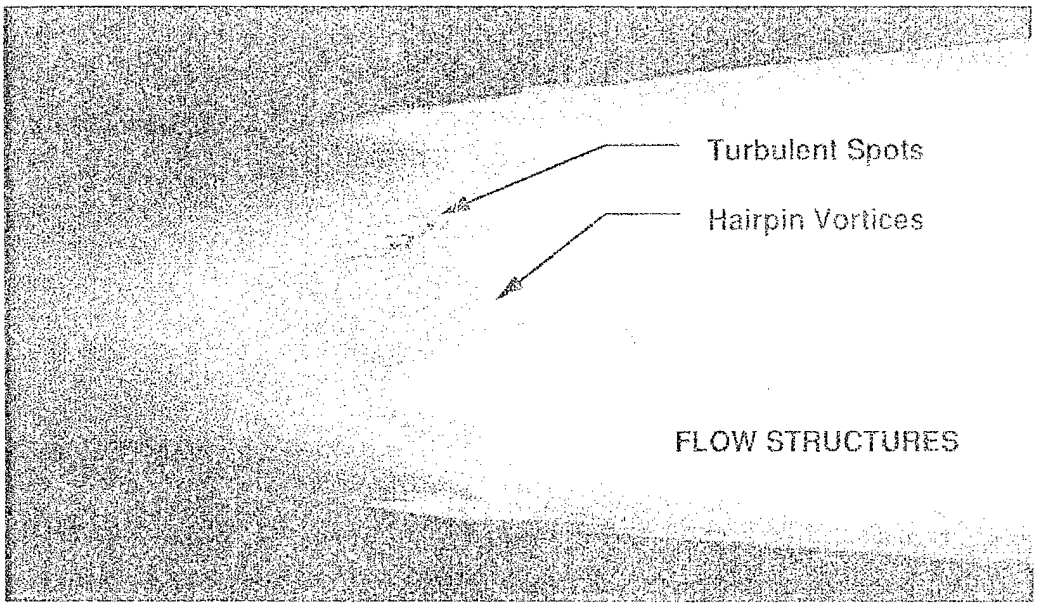


Figure 1 Visualization of the transition process on an axisymmetric body operating underwater.[5]

The streamwise distance between the point (at $x_1 = x_o$) in the laminar layer where spots first occur and the beginning of the TBL is called the *transition length*, $\Delta x$. The *transition region* (or *zone*) is the area covered by turbulent spots, e.g., $L_3\ \Delta x$, where $L_3$ is the spanwise extent of spot existence. A small pressure transducer located within the transition region generates a signal, $p_{trans}(x_1,x_3,t)$, that is *intermittent* - a signal that signifies laminar flow behaviour at some instants of time, and turbulent flow behaviour at all other instants. The percentage of time that the flow is turbulent at some given in-plane location $(x_1,x_3)$ within the transition region, as determined from a time average of the intermittent signal, is called the *intermittency factor*, $\gamma(x_1,x_3)$. The intermittent pressure (or velocity or wall shear stress) signal measured in the transition zone can be conditioned electronically[6] to form the intermittency *indicator function*, $I(x_1,x_3,t)$. The indicator function is a zero-one function; zero when the flow is laminar, and one when the flow is turbulent. Clearly, the time average of $I(x_1,x_3,t)$ is $\gamma(x_1,x_3)$. The *burst rate*, $N(x_1,x_3)$ is the average number of turbulent spots per unit time that pass the given in-plane location. Figure 2 schematically illustrates these concepts for a given spanwise position, $x_3$ = constant.

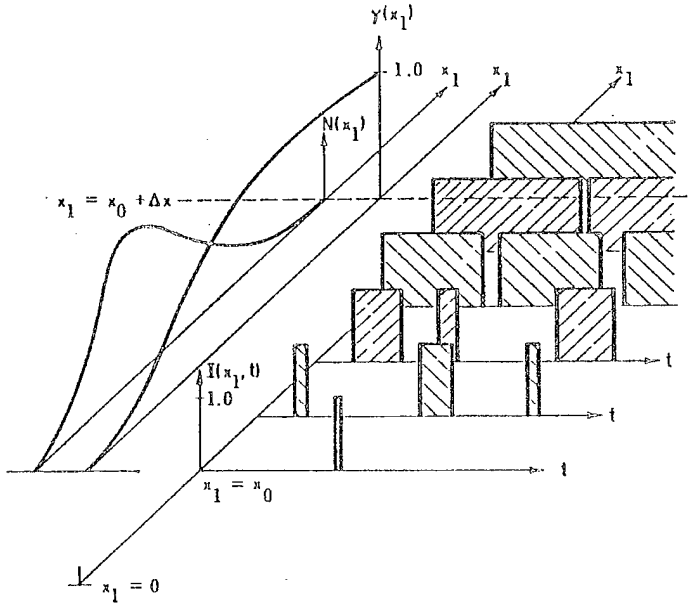


Figure 2 Intermittency indicator function, $I(x_1,t)$, the burst rate, $N(x_1)$, and the intermittency factor, $\gamma(x_1)$ for some fixed spanwise location in the transition region.

## A. Intermittency statistics for boundary-layer transition

Josserand and Lauchle[7] measured the space-time correlation functions of $I(x_1,x_3,t)$ as it occurs naturally in a zero-pressure gradient, flat plate boundary-layer transition zone. They also derived empirical models to describe these correlation functions. If the plate can be considered as infinite in the transverse direction, it is reasonable to let statistical averages of $I(x_1,x_3,t)$ be independent of $x_3$; however, they are nonhomogeneous in $x_1$ direction. The definition of coordinate symbols[7] to be used here are given in Figure 3. The time-average value of the intermittency indicator function is the intermittency factor defined as:

$$\gamma(x_1) = \lim_{T\to\infty} \frac{1}{T}\int_0^T I(x_1,x_3,t)dt \,. \tag{1}$$

Josserand and Lauchle[7] investigated the intermittency factor and described the experimental results as:

$$\gamma(Z_1) = 1 - e^{-(C_3 - C_4 Z_1)Z_1^2}, \tag{2}$$

where $z_1 = (x_1-x_o)/\Delta x \equiv \eta_1/\Delta x$, and $C_3$ and $C_4$ are, respectively, 1.0 and 3.4.

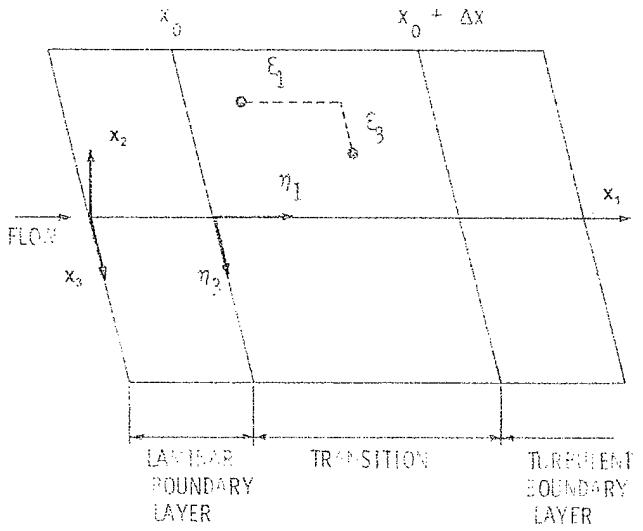


Figure 3 Definition of coordinates.

Another important statistical property of the intermittency is the spot rate $N(x_1)$. It is described as the mean number of spots that occur at a given streamwise point per unit time. As like the intermittency factor, it is assumed independent of $x_3$. The non-dimensionalization of the spot rate was first suggested by Farabee et al.[8] and later modified by Gedney and Leehey,[9] i.e.,

$$N^*(z_1) = 0.420\left(\frac{\Delta x}{U_\infty}\right) N(z_1). \tag{3}$$

Josserand and Lauchle[7] also found that their experimental data is well described by the Dirac line source hypothesis,[9]

$$N^*(z_1) = C_5\sqrt{(1-\gamma)ln\left(\frac{1}{1-\gamma}\right)} \tag{4}$$

with $C_5 = 2.38U_\infty/\Delta x$.

The indicator function process is assumed to be independent of that governing the velocity or pressure fluctuations within a single turbulent patch. It is further assumed that the statistics within the patch or spot of turbulence is analogous to that under the fully-developed TBL. Therefore, the wall pressure correlation function during transition is modeled as the product of the correlation function of the indicator function, $R_I$ with that of the TBL, $R_{Turb}$ :

$$R_{trans}(\eta_1,\xi_1,\xi_3,\tau) = E\{p_{trans}(\eta_1,\eta_3,t)p_{trans}(\eta_1+\xi_1,\eta_3+\xi_3,t+\tau)\}$$
$$= R_I(\eta_1,\xi_1,\xi_3,\tau)R_{Turb}(\xi_1,\xi_3,\tau)\,. \tag{5}$$

An empirical model[7] to describe the indicator correlation function is:

$$R_I(\eta_1,\xi_1,\xi_3,\tau) = \gamma_u\gamma_d + \gamma_u(1-\gamma_d)exp\left\{-5\left(4+200\left|\tau-\frac{\xi_1}{U_c}\right|\right)\left|\tau-\frac{\xi_1}{U}\right|\right\}$$
$$exp\left(20\frac{|\Lambda_1|}{0.014+|\Lambda_1|}\left|\tau-\frac{\xi_1}{U}\right|\right)$$
$$exp\left(-\left|15.75\Delta x-\frac{1260\left|\tau-\frac{\xi_1}{U}\right|}{1+71|\Lambda_3|}\right|\frac{|\Lambda_3|}{1+14.2|\Lambda_1|}\right) \tag{6}$$
$$exp\left(-\frac{A|\Lambda_1|}{0.0014+|\Lambda_1|}\frac{1}{1+1300\left|\tau-\frac{\xi_1}{U_c}\right|}\right).$$

Here, subscript $u$ refers to the upstream sensor location and $d$ to the downstream sensor location, $\Lambda_1$ ($\Lambda_3$) = $\xi_1$ ($\xi_3$)/$\Delta$x, A = -*ln*[1-exp(-4.27/$\Delta$x)] with $\Delta$x in meters, and

$$\gamma_u = \gamma(\eta_1) \quad and \quad \gamma_d = \gamma(\eta_1+\xi_1)$$

when the reference sensor location is upstream of the second sensor. For these positions reversed, we have:

$$\gamma_u = \gamma(\eta_1+\xi_1) \quad and \quad \gamma_d = \gamma(\eta_1)\,.$$

## II. THE WAVEVECTOR-FREQUENCY SPECTRUM FOR BOUNDARY-LAYER TRANSITION WALL PRESSURE FLUCTUATIONS

For the homogeneous field signal, wavevector spectrum analysis is a very powerful tool to identify the characteristics of the signal. For the infinitely wide plate, the transition zone statistics are homogeneous in the spanwise direction. But by its very nature, boundary layer transition has

statistics that are inhomogeneous in the streamwise direction. This is because the statistically averaged flow variables change from those of a laminar state to those of a turbulent one. This stochastic process is described formally as one that is *weakly non-homogeneous*. Analogously to time-frequency analysis for a weakly non-stationary temporal process, where waterfall analysis may be utilized, wavevector-frequency spectral analysis (with varying reference position) may be used in the weakly non-homogeneous process. This analysis can capture the wavenumber and frequency spectral changes throughout the field. Such information helps us to understand more thoroughly the ways in which boundary layer transition can act as a pressure forcing function to real structures that may respond dynamically to the effects of the induced wall pressure fluctuations.

### A. Implementation

The wall pressure wavevector-frequency spectrum for the transition zone wall pressure fluctuations can be calculated directly from Equation (5) by Fourier transforming over both space and time. In particular, we find:

$$\Phi_{rs}^{Tran}\left(\eta_1, k_1, k_3, \omega\right) = \Phi_{rs}^{I}\left(\eta_1, k_1, k_3, \omega\right) * \Phi_{rs}^{Turb}\left(k_1, k_3, \omega\right). \tag{7}$$

The asterisk symbol indicates convolution of the transition zone intermittency indicator function spectrum with that of a fully-developed TBL. Subscript $r$ refers to the reference sensor and $s$ to the second sensor. For the indicator function:

$$\Phi_{rs}^{I}\left(\eta_1, k_1, k_3, \omega\right) = \frac{1}{(2\pi)^3}\int_{-\infty}^{+\infty}\int_{-\infty}^{+\infty}\int_{-\infty}^{+\infty} R_I\left(\eta_1, \xi_1, \xi_3, \tau\right) e^{-i\left(k_1\xi_1 + k_3\xi_3 - \omega\tau\right)}\, d\xi_1\, d\xi_3\, d\tau\,. \tag{8}$$

The TBL wavevector-frequency spectrum is relatively well known and can be obtained from many different sources in the contemporary literature. We use the Corcos[10] model because of its simplicity and ease of implementation. To calculate the wall pressure wavevector-frequency spectrum in the transition zone from Equation (7), we need to first substitute Equation (6) into Equation (8) and evaluate the transform.

### B. Indicator function wavevector-frequency spectrum

The dual relationship between the space-time correlation function and the wavevector-frequency spectrum is the three-dimensional Fourier transform given by Equation (8). In this research, numerical processing is performed spanwise and streamwise, separately. Therefore, only two-dimensional Fourier transforms are required (one in space and one in time), which leads to two separate *wavenumber*-frequency spectra. For the streamwise direction, we have:

$$\Phi_I\left(\eta_1, k_1, \omega\right) = \frac{1}{(2\pi)^2}\int_{-\infty}^{+\infty}\int_{-\infty}^{+\infty} R_I\left(\eta_1, \xi_1, 0, \tau\right) e^{-i\left(k_1\xi_1 - \omega\tau\right)}\, d\xi_1\, d\tau\,, \tag{9}$$

and for the spanwise direction:

$$\Phi_2(\eta_1, k_3, \omega) = \frac{1}{(2\pi)^2} \int_{-\infty}^{+\infty} \int_{-\infty}^{+\infty} R_1(\eta_1, 0, \xi_3, \tau)\, e^{-i(k_3\xi_3 - \omega\tau)}\, d\xi_3\, d\tau \,. \tag{10}$$

Accurate numerical evaluation of these transforms requires that the limits of integration be truncated to finite values, and that the sampling functions are chosen to prevent aliasing in both the frequency and wavenumber domains. Because the space-time correlation functions are developed from experimental data[7] collected in air over a given finite area of a test plate, the spatial limits and increments are chosen to correspond to those of the experimental transducer array. That is, $\Delta\xi_1 = \Delta\xi_3 = 2.54$ cm. These uniform spatial sampling increments result in un-aliased wavenumber spectra[11,12] for $k_1$ ($k_3$) $\leq \pi/\Delta\xi_1(\Delta\xi_3)$, i.e., $|k_1,k_3| \leq 123$ rad/m. In accordance to the experimental array size, 41 spatial samples are chosen in the stream and spanwise directions. The temporal sampling frequency is set at 250 Hz, which results in un-aliased frequency domain spectra for $f < 125$ Hz.

The correlation values computed from Equation (6) must approach zero smoothly as the limits of integration are exceeded. This is accomplished by *windowing*. In the transformed domains, the selected window function should have low sidelobes in order to minimize sidelobe leakage into the spectral results that can distort the true wavenumber content of the pressure fluctuations. This can be accomplished with many window functions, but at the cost of broadening the mainlobe. This diminishes the spectral resolution. Because this research involves the pressure field of an intermittent turbulent layer, known to contain broadband energy levels, but concentrated in specific regions of the wavenumber-frequency domain, the resolution issue is deemed less important than the sidelobe leakage problem. Therefore, a Taylor weighting function[11,13] was used, for both the spatial and temporal windows. This weighting function is

$$w(p) = \frac{1}{2\pi}\left\{F(0) + 2\sum_{m=1}^{\bar{n}-1} F(m)\cos(mp)\right\}, \quad |p| \leq \pi$$

$$F(m) = \prod_{n=1}^{\bar{n}-1} 1 - \frac{\dfrac{m^2}{\sigma^2\left(A^2 + \left(n - \frac{1}{2}\right)^2\right)}}{1 - \dfrac{m^2}{n^2}} \frac{\sin(\pi m)}{\pi m} \tag{11}$$

$$\sigma = \frac{\bar{n}}{\sqrt{A^2 + \left(\bar{n} - \frac{1}{2}\right)^2}}, \quad A = \frac{1}{\pi} ln\left(R + \sqrt{R^2 - 1}\right), \quad R = 10^{\frac{|S|}{20}} \,.$$

Taylor weighting is known to make the first few sidelobes near the mainlobe nearly flat.[13] The parameter S controls the sidelobe level in dB, and the parameter n controls the number of the nulls. We choose S = 60 dB and n = 2.

The windowing operation effectively suppresses sidelobe leakage, but it also introduces the unavoidable effect of spectral amplitude reduction. A window calibration factor is thus used to preserve the original power of the signal. This is explained qualitatively as follows. If both the reference and second probe are located under the TBL, then the indicator function is unity and the two-dimensional FFT of this function would be a product of two unit delta functions. When convolved with the TBL spectrum, according to Equation (7), we obtain the desired result: the wavevector-frequency spectrum of the TBL wall pressure fluctuations. But, if we perform this process with a window, the two-dimensional FFT of the windowed indicator function mimics a pair of delta functions, but they have magnitudes greater than unity (by about 1.4%). Consequently, the convolution results in a magnitude error for the TBL spectrum. A narrowband window calibration factor is thus required to compensate for this effect. This factor is calculated in the wavenumber-frequency domain to preserve the overall magnitude of the original signal. First, a two-dimensional FFT is performed on the Taylor window function, and the sum of the values in each wavenumber (or frequency) bin is compared with the two-dimensional FFT for a uniform function of unit amplitude. The ratio of these two computations is then multiplied, bin-by-bin, with the required two-dimensional FFT's calculated using the window.

### C. Transition zone wall pressure spectrum

The wavenumber-frequency spectrum of the wall pressure fluctuations under the transition zone is calculated from the convolution described by Equation (7), using the Taylor windowed spectrum of the indicator function. In the streamwise direction, we have:

$$\Phi_{Trans}\left(\eta_1, k_1, \omega\right) = \Phi_1\left(\eta_1, k_1, \omega\right) * \Phi_{Turb}\left(k_1, \omega\right) \tag{12}$$

and, for the spanwise direction:

$$\Phi_{Trans}\left(\eta_1, k_3, \omega\right) = \Phi_2\left(\eta_1, k_3, \omega\right) * \Phi_{Turb}\left(k_3, \omega\right) \ , \tag{13}$$

where the $\Phi_{1,2}$ spectra are computed using the procedures of Section II.B. The Corcos (1964) models for the TBL wall pressure wavenumber-frequency spectra are:

$$\Phi_{Turb}\left(k_1, \omega\right) = \frac{L_1 \, \Phi(\omega) / \pi}{1 + L_1^2\left(k_1 - k_c\right)^2} \ , \qquad \Phi_{Turb}\left(k_3, \omega\right) = \frac{L_3 \, \Phi(\omega) / \pi}{1 + L_3^2 \, k_3^2} \ , \tag{14}$$

where $\Phi(\omega)$ is the point wall pressure spectrum, and the correlation lengths are:

$$L_1 = \frac{u_c}{\varepsilon_1 \omega} \ , \quad L_3 = \frac{u_c}{\varepsilon_3 \omega} \ , \quad \varepsilon_1 = 0.11 \ , \ \varepsilon_3 = 0.71 \ . \tag{15}$$

## III. RESULTS

Calculations are performed in MATLAB.® where the 2-D FFT and convolution operations are functions provided in this software package. Figure 4 shows the streamwise space-time correlation function of the indicator function calculated using Equation (6) and $\xi_3 = 0$. These

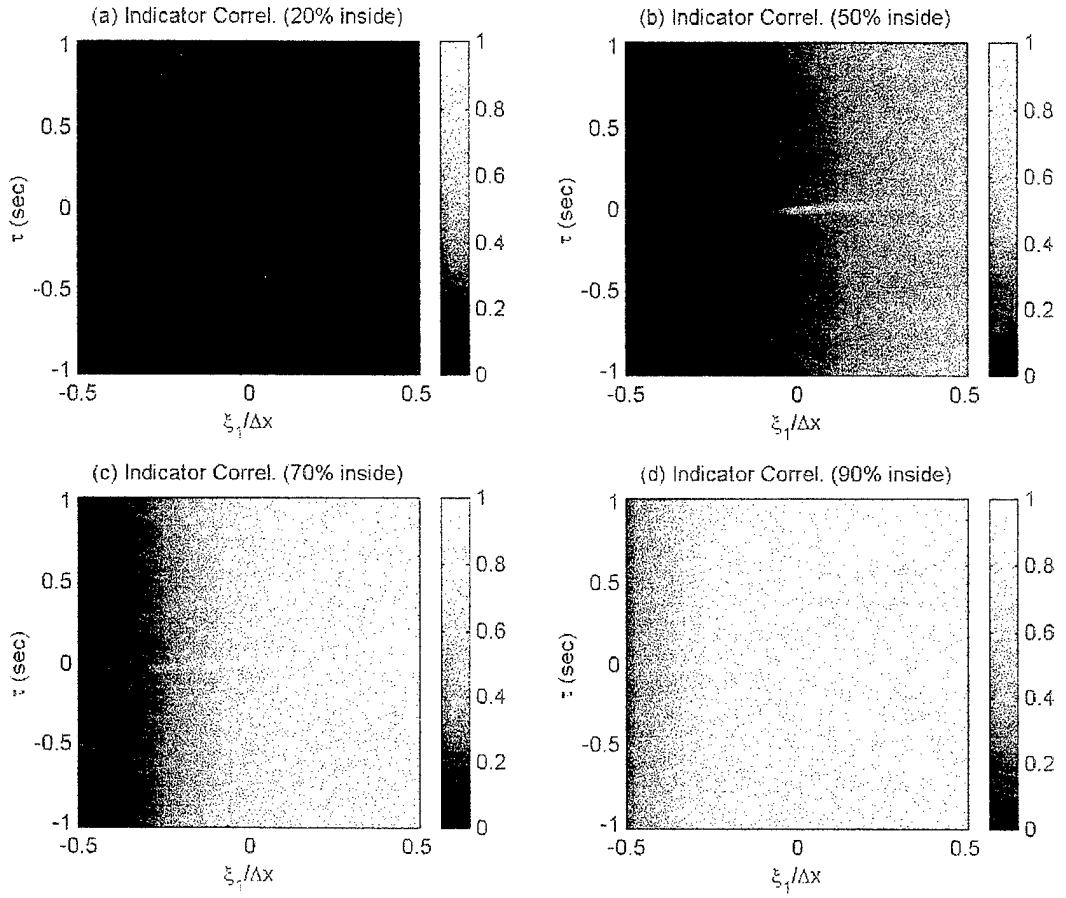


Figure 4 Calculated streamwise space-time correlation functions for transition zone intermittency function, $R_I(\eta_1,\xi_1,0,\tau)$ with $0.2 \le z_1 \le 0.9$.

correlations are shown for four (4) reference positions within $0.2 \le z_1 \le 0.9$. The temporal variable ranges from -1 s to 1 s with a time increment of 4 ms, and the spatial variable ranges from 0.508 m upstream to 0.508 m downstream in 2.54 cm increments. This range encompasses the entire transition zone measured by Josserand and Lauchle[7] at a free-stream velocity of 11.77 m/sec (in air). At large delay times the correlation function approaches $(\gamma_r\gamma_s)^{1/2}$, so the color contrast of the plots at the upper and lower borders follow the same functional behavior as $\gamma_s$ through the range of $\xi_1$, weighted by the value of $\gamma_r$. This is further indicated by the plots becoming lighter as we progress from $z_1 \sim 0$ to $z_1 \sim 1$.

At each reference position, the wavenumber-frequency spectrum is calculated, Figure 5.

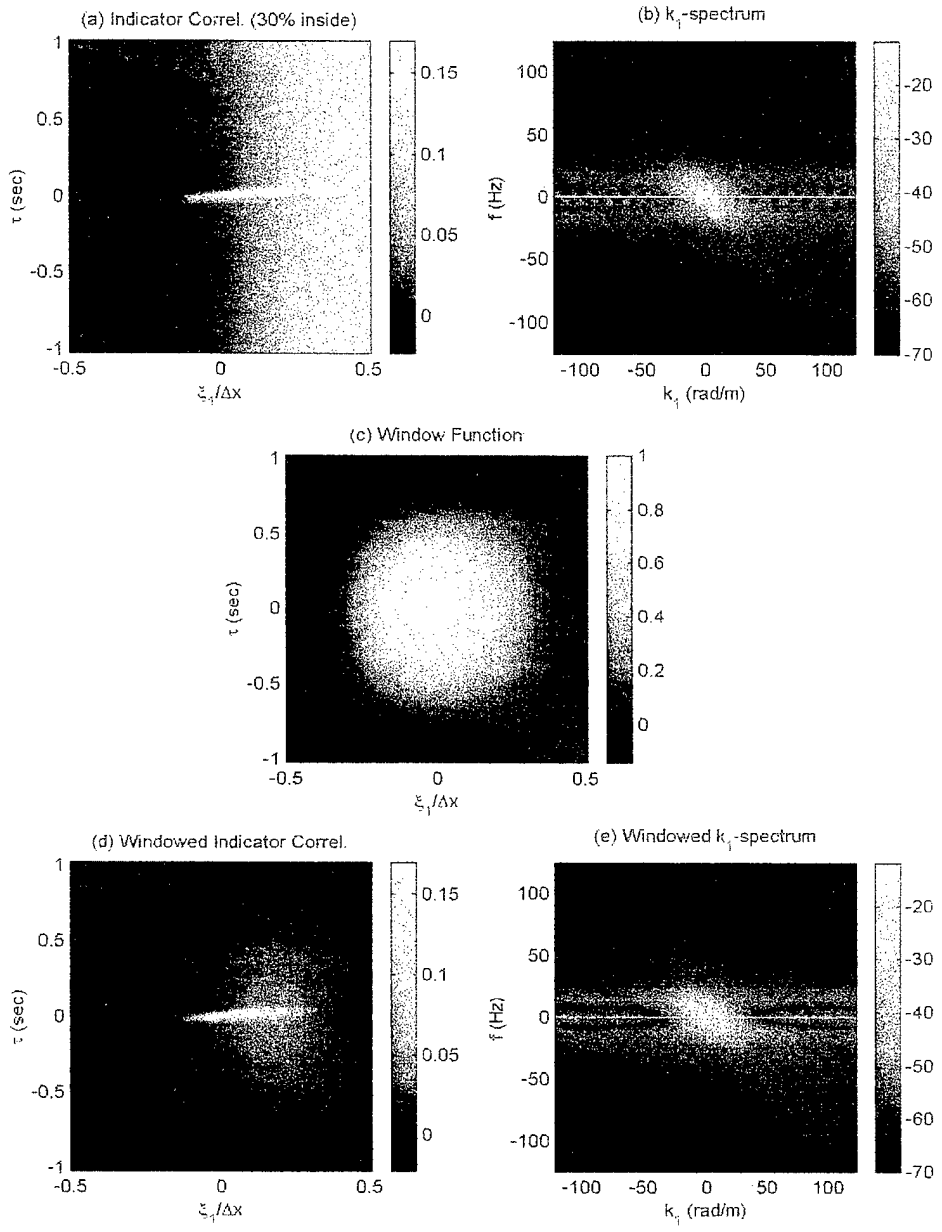


Figure 5 Processing steps for calculating the streamwise wavenumber-frequency spectrum (for $z_1 = 0.3$): (a) space-time correlation function for the indicator function: (b) 2-D FFT of correlation shown in (a); (c) the Taylor weighting function; (d) correlation function for the indicator function after application of the Taylor window: (e) streamwise wavenumber-frequency spectrum of the indicator function after the necessary windowing operation.

For a reference position that is 30% into the transition zone, Figure 5(a) shows the correlation function for the indicator function, and 5(b) shows the streamwise wavenumber-frequency transformation of this function with no windowing operation performed. The space-time characteristics of the Taylor window function, Equation (11), is shown in Figure 5(c). Now when this window function is multiplied by the indicator correlation function, a windowed indicator correlation function is created as shown in Figure 5(d). The streamwise wavenumber-frequency spectrum of this windowed indicator function is shown in Figure 5(e). The suppression of sidelobe leakage, in *both* frequency and wavenumber, through use of the window function is clearly observed when comparing Figure 5(b) to 5(e).

In Figure 6 we compare the wavevector-frequency spectra for the fully-developed TBL with that of the transition zone at a reference location 30% into the zone. The flow conditions are

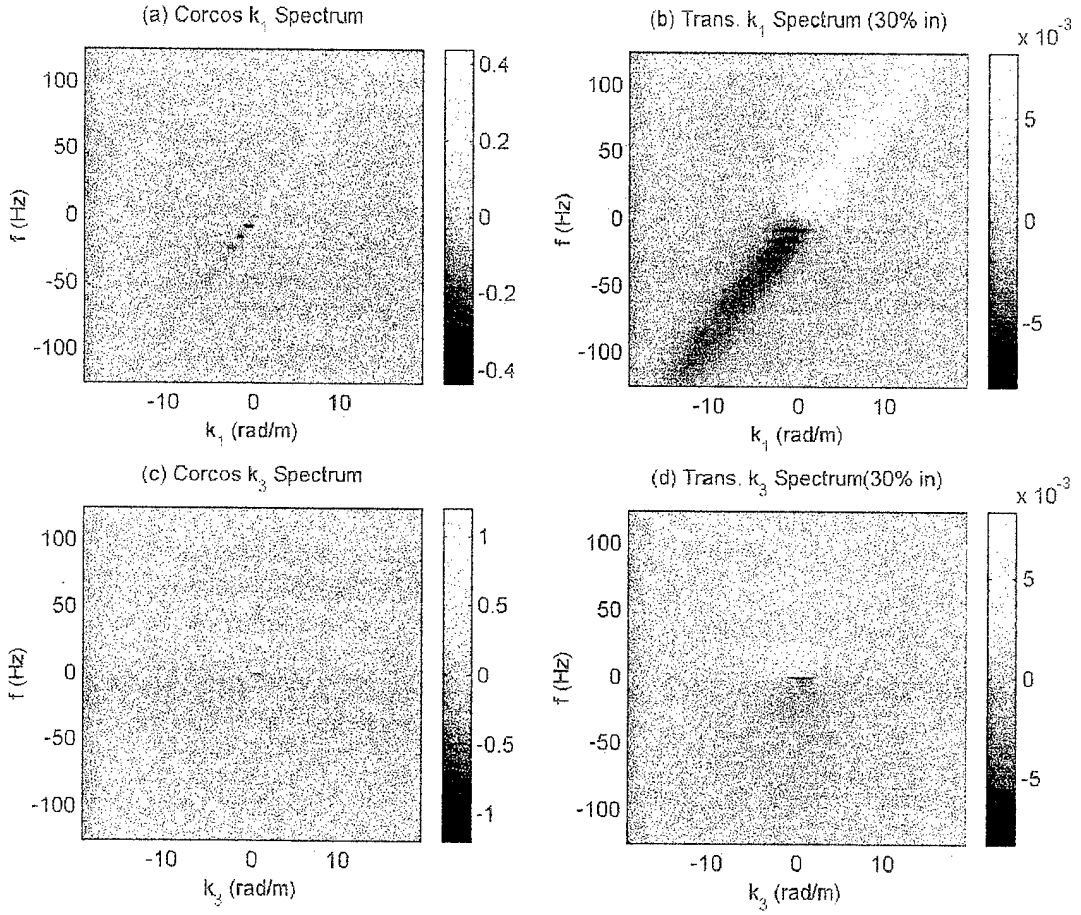


Figure 6 Turbulent boundary layer wall pressure wavevector-frequency spectrum[10] [m/rad] compared to that under a transitional boundary layer on a flat plate operating at zero incidence in air at 11.77 m/s: (a) $k_1$-$\omega$ spectrum of the TBL; (b) $k_1$-$\omega$ spectrum for transition; (c) $k_3$-$\omega$ spectrum of the TBL; (d) $k_3$-$\omega$ spectrum for transition.

assumed identical for each of these calculations, the levels are normalized by $\Phi(\omega)$, so the spectrum levels presented here have the units of meters per radian. Equation (14) is used for Figures 6(a) and (c), while Equations (12) and (13) are used for 6(b) and (d), respectively. The Taylor window is applied throughout. There is apparently higher low-wavenumber energy created in the transition zone than in the TBL as indicated by lighter highlights along the convective ridge in the $\omega$-$k_1$ plots. This feature can be visualized easier by cross-plotting the spectrum level at constant frequency with wavenumber.

Figure 7 shows the non-dimensionalized $k_1$-$\omega$ spectra for both the TBL and the transition zone at various reference locations, and for four (4) discrete frequencies [the spectrum level is normalized with $\Phi(\omega)/k_c$]. As the reference position moves downstream, the low $k_1$-wavenumber spectral content increases over that of the TBL. This effect is observed for all of the considered frequencies, but it is especially noticeable at the lower frequencies.

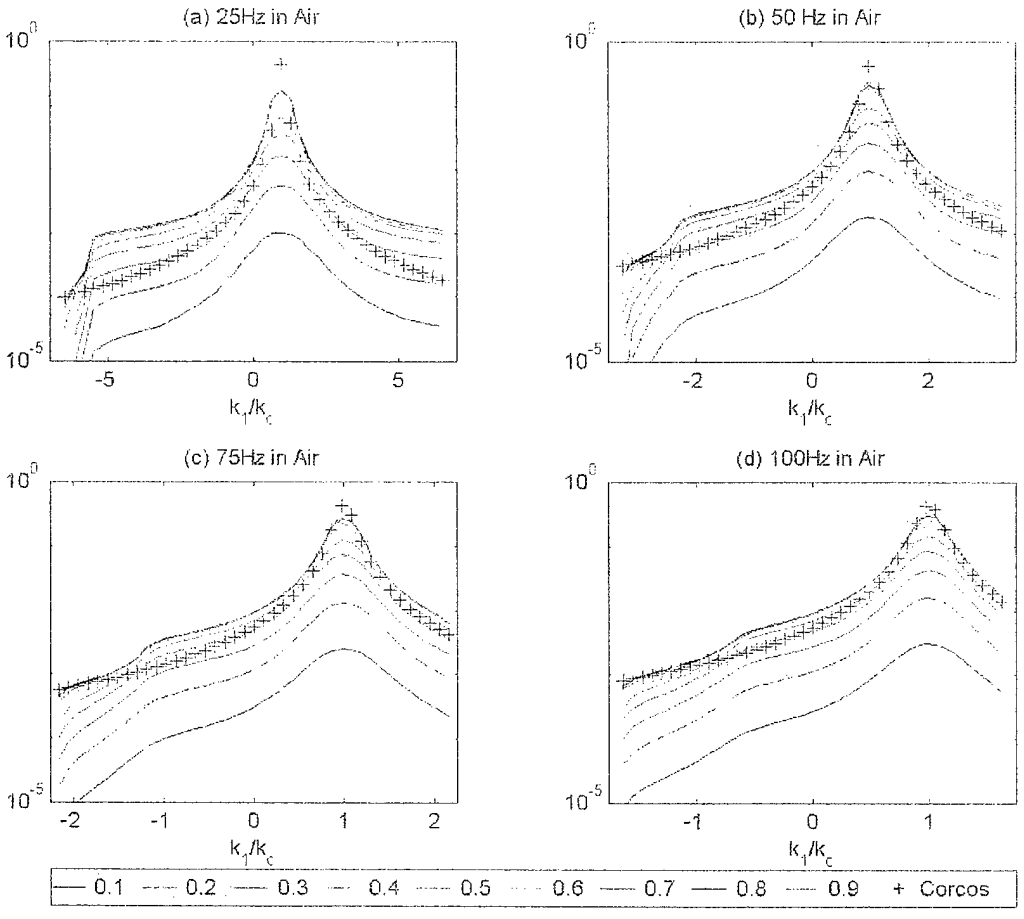


Figure 7 Non-dimensional $k_1$-$\omega$ spectra at various frequencies, and for $0.1 \le z_1 \le 0.9$: ++++++ indicates the TBL wavenumber spectrum;[10] frequencies (a) 25 Hz; (b) 50 Hz; (c) 75 Hz; (d) 100 Hz.

In Figure 8, we show the spanwise wavenumber spectra at the four (4) constant frequencies in the same format as Figure 7. Clearly, the transition zone wall pressure $k_3$-$\omega$ spectrum is virtually identical to that of the fully-developed TBL for $z_1 = 0.9$. For smaller values of $z_1$, the transition zone spectral levels decrease in proportion to the intermittency factor.

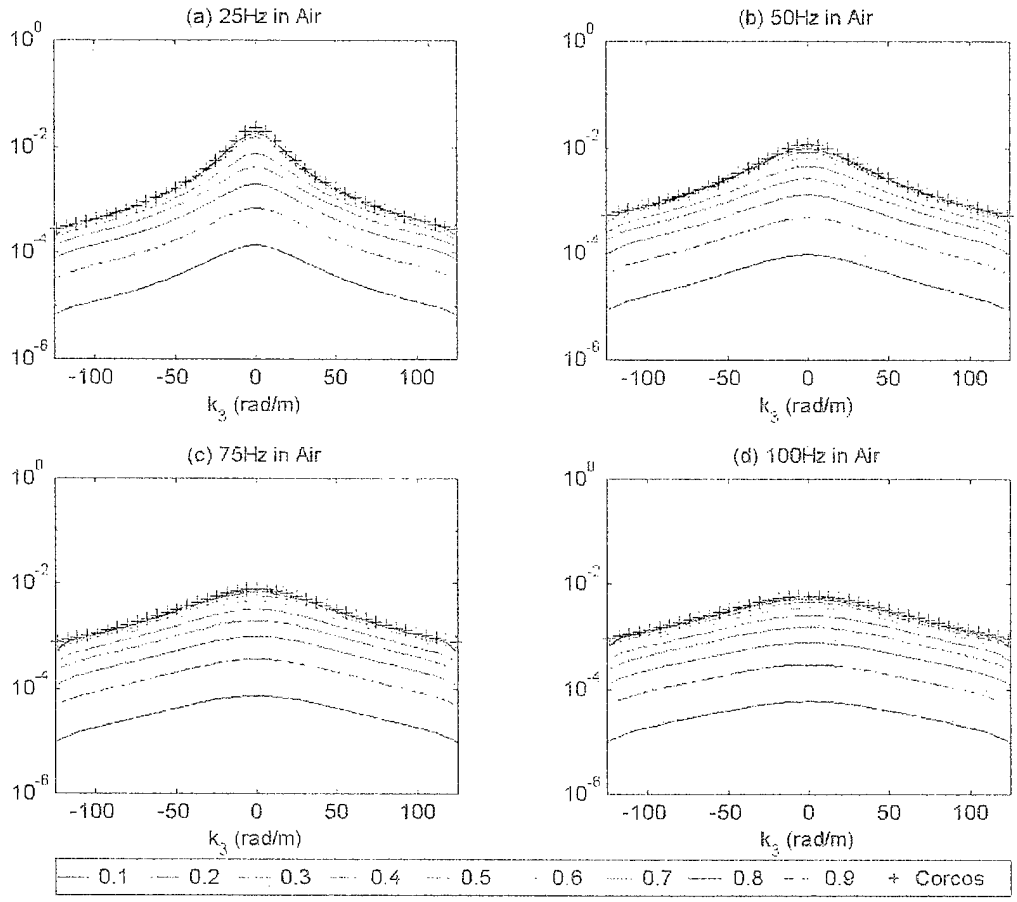


Figure 8 Spanwise wavenumber spectra [m/rad] at various frequencies for $0.1 \le z_1 \le 0.9$: ++++++ indicates the TBL wavenumber spectrum:[10] frequencies (a) 25 Hz: (b) 50 Hz: (c) 75 Hz: (d) 100 Hz.

## A. Discussion

As described qualitatively by Kadanoff.[14] energy in turbulent flows *cascades* from large scales to small scales. The largest scales of the flow exist in the *integral range*. It is in this range where the initial disturbances that cause the flow to exist take place - the Fourier components of the pressure or velocity are of very low wavenumber: $|k_1| << k_c$. The initial energy then cascades into the *inertial range*, where intermediate scales of the flow exist, and $|k_1| \le k_c$. Finally, the energy

dissipates in the *viscous range* of very small scales and large wavenumbers: $|k_1| > k_c$. In the terminology of Kolmogorov turbulence theory, *intermittency* describes the degree of fluctuation in the turbulent field. The theory suggests that higher intermittency results in higher inertial range energy levels.

In the context of boundary-layer transition, intermittency also means fluctuation, but its peak-to-peak magnitude is considerably higher than the typical fluctuation level of the TBL. In the transition zone, the minimum fluctuation level is that of the laminar flow state, while the maximum is that of the turbulent state. So, within the transition zone, we would expect higher wall pressure fluctuation levels in the inertial range where $|k_1| \leq k_c$. The $k_1$-$\omega$ spectra of the transition zone wall pressure fluctuations presented here indicate that the low-wavenumber components are higher than those of a TBL that might exist superficially at the same location and Reynolds number. The increase occurs when $z_1 \geq 0.5$ which happens to correspond to the peak in the burst rate distribution [$N(x_1)$, Equation (4)]. The peak in the burst rate would imply a more energetic state, of higher intermittency, and hence, of higher level low-wavenumber pressure fluctuation. This effect is not only borne out by the calculations presented here, but also by the experimental results of Audet, et al[15] and Dufourcq[16] as reproduced in Figure 9. The figure shows the local rms wall pressure fluctuations measured under a flat plate boundary-layer transition zone, as a function of streamwise position. The peak occurs approximately 50% into the zone which offers subjective proof of the intermittency hypothesis offered here.

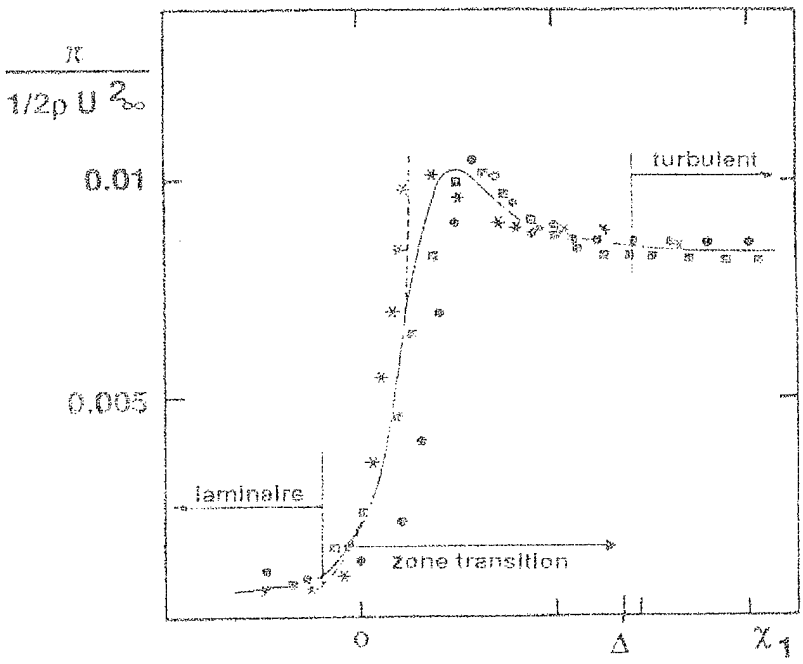


Figure 9 Local rms wall pressure fluctuations measured under a transitional boundary layer on a flat plate (from Audet, et al[15] and Dufourcq[16]).

In addition to the intermittency mechanism is one of *discontinuous turbulence*. Turbulence exists only within the spots during transition. Therefore, packets of pressure waves propagate along the flow surface at various speeds ~ $\omega/k_1$. For illustrative purposes, consider constant $\omega$ and $k_1 = k_c$. Under the fully-developed TBL, the wave packet is actually a long traveling wave as modeled by the simple sine wave shown in Figure 10(a). The wave packet associated with a turbulent spot is a modulated traveling wave as modeled in Figure 10(b).

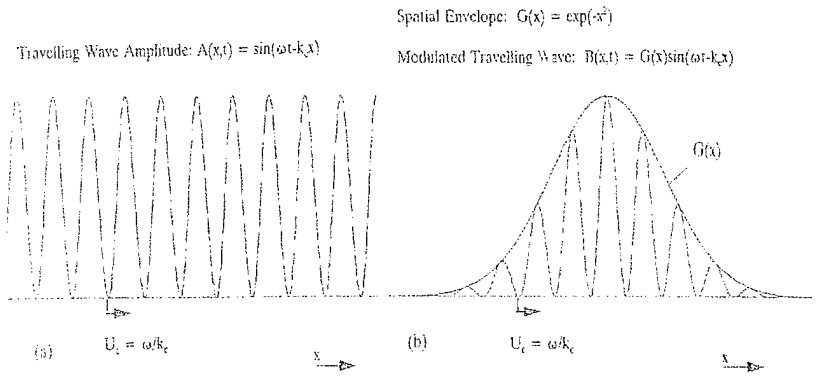


Figure 10 Simple concepts of (a) a traveling wave and (b) a propagating wave packet.

Performing a Fourier transform on the two analytical functions shown in Figure 10 results in the wavenumber spectra shown in Figure 11. The traveling wave has only a single wavenumber component at $k_1 = k_c$. The modulated traveling wave, however, generates a continuous spectrum of wavenumbers. The low-wavenumber content of an intermittent, discontinuous wall pressure field would therefore be expected to be higher than that of a continuous one.

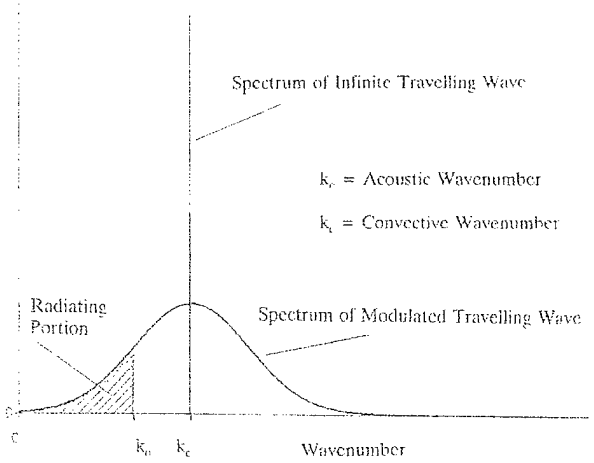


Figure 11 $k_1$ spectra computed for a traveling wave and a wave packet of frequency $\omega$.

## IV. CONCLUSIONS

In this paper we have used existing space-time correlations for the intermittency function[7] that describe the growth and coalescence of turbulent spots in a naturally occurring subsonic boundary-layer transition zone to model the wavevector-frequency spectrum of the transition zone wall pressure fluctuations. The theory assumes that the space-time characteristics of the wall pressure fluctuations within individual spots follow the Corcos[10] model for pressure fluctuations under a fully-developed turbulent boundary layer, and that this process is statistically independent of the indicator function process. The wavevector-frequency spectrum of the transition zone wall pressure fluctuations is thus the convolution of the wavevector-frequency spectrum of the intermittency function with that of the TBL wall pressure fluctuations.

Comparisons of the wavevector-frequency spectrum of the transition zone wall pressure fluctuations with that of the TBL, assumed to exist at the same location and flow conditions, reveal the following observations and conclusions:

1. At a fixed frequency, the low-streamwise wavenumber wall pressure components under transition are larger than those under the TBL for transition zone statistical reference locations greater than $0.5\Delta x$, where $\Delta x$ is the transition length.

2. At the same fixed frequencies, the spanwise wavenumber wall pressure components are less than or equal to those of the TBL, depending on the reference location.

3. The higher spectral levels for streamwise wavenumbers that are less than the convective wavenumber are attributed to two physical mechanisms: high turbulence intermittency in the inertial energy range, and discontinuous turbulence due to the spot formation process.

4. The engineering relevance of these findings is that the wall pressure fluctuations induced by transitional boundary layers may act as efficient forcing functions to real structures that support resonant frequencies and flexural wavenumbers that fall within the low-wavenumber region of the subject calculations. The directly radiated sound from the transition zone may also be greater than that of a TBL of equal area. The fluid-structure coupling and direct radiation from transition could result in increased structural vibration, far-field radiation, and sensor self noise, for sensors mounted in the structure.

## REFERENCES


1. Howe, M. S. *Acoustics of Fluid-Structure Interactions*. Cambridge University Press, London (1998).

2. Blake, W. K. *Mechanics of Flow-Induced Sound and Vibration, Volumes I and II.* Academic Press, Orlando (1986).

3. Farabee, T. M. An Experimental Investigation of Wall Pressure Fluctuations Beneath Non-Equilibrium Turbulent Boundary Layers. Ph.D. Thesis, Catholic University of America (1986).

4. Lauchle, G. C. Hydroacoustics of Transitional Boundary-Layer Flow. *Appl. Mech. Rev.* **44**:517-531 (1991).

5. Lauchle, G. C., H. L. Petrie, D. R. Stinebring. Laminar Flow Performance of a Heated Body in Particle-Laden Water. *Exp. in Fluids* **19**:305-312 (1995).

6. Lauchle, G. C., G. B. Gurney. Laminar Boundary-Layer Transition on a Heated Underwater Body. *J. Fluid Mech.* **144**:79-101 (1984).

7. Josserand, M. A., G. C. Lauchle. Modeling the Wavevector-Frequency Spectrum of Boundary-Layer Wall Pressure During Transition on a Flat Plate. *Trans. ASME - J. Vib. and Acoust.* **112**:523-534 (1990).

8. Farabee, T. M., M. J. Casarella, F. C. DeMetz. Source Distribution of Turbulent Bursts During Natural Transition. David W. Taylor Naval Ship Research and Development Center, SAD 89E,1942 (1974).

9. Gedney, C. J., P. Leehey. Wall Pressure Fluctuations During Transition on a Flat Plate. *Trans. ASME J. Vib. And Acoust.* **113**: 255-266 (1991).

10. Corcos, G. M. The Structure of the Turbulent Pressure Field in Boundary Layer Flows. *J. Fluid Mech.* **18**: 353-378 (1964).

11. Ochsenknecht, R. I. Estimation of the Wavenumber-Frequency Spectra for the Non-Homogeneous Streamwise Transition Flow Pressure Field. Master of Science Thesis, Penn State University (1996).

12. Strawderman, W. A. *Wavevector-Frequency Spectra with Applications to Acoustics.* U.S. Government Printing Office, Washington, DC 20402 (undated).

13. Streit, R. L. A Discussion of Taylor Weighting for Continuous Apertures. Naval Underwater Systems Center TM 851004, New London, CT (1985).

14. Kadanoff, L. P. A Model of Turbulence. *Physics Today*, September 1995, pp. 11-13.

15. Audet, J., Dufourcq, Ph., Lagier, M. Pression Pariétale sous une Couche Limite lors de la Transition vers la Turbulence. *J. Acoustique* 2: 369-378 (1989).

16. Dufourcq, Ph. Influence d'un Écoulement de Type Couche Limite sur la Localisation de Sources Sonores Placées en Paroi. Doctoral Thesis, Ecole Centrale de Lyon (1984).

**DISTRIBUTION LIST FOR ARL PENN STATE TM00-100 BY G. C. Lauchle and S. Park, dated 18 May 2000.**

Commander
Office of Naval Research
800 N. Quincy Street
Arlington, VA 22217-5660
Attn: K. Ng, Code 333
Copy No. 1

Office of Naval Research
Attn: Jan Lindberg, Code 321SS
Copy No. 2

Office of Naval Research
Attn: Patrick Purtell, Code 334
Copy No. 3

Office of Naval Research
Attn: J. F. McEachern, Code 321SS
Copy No. 4

Office of Naval Research
Attn: S. Lekoudis, Code 333
Copy No. 5

Office of Naval Research
Attn: G. Jebsen, Code 334
Copy No. 6

Office of Naval Research
Attn: E. Rood, Code 334
Copy No. 7

DARPA
3701 N. Fairfax Drive
Arlington, VA 22203-1714
Attn: James McMichael
Copy No. 8

Naval Surface Warfare Center
Carderock Division
9500 MacArthur Boulevard
West Bethesda, MD 20817-5700
Attn: T. Farabee, Code 7250
Copy No. 9

Naval Surface Warfare Center
Carderock Division
Attn: W. K. Blake
Copy No. 10

Naval Sea Systems Command
2531 Jefferson Davis Highway
Arlington, VA 22242-5160
Attn: Jim Fein
Copy No. 11

CNO Executive Panel
4401 Ford Avenue
Alexandria, VA 22302-0268
Attn: Scott Littlefield
Copy No. 12

Naval Undersea Warfare Center Division,
Newport
1176 Howell Street
Newport, RI 02841-5047
Attn: P. J Lefebvre, Bldg. 990/5
Copy No. 13

Naval Undersea Warfare Center Division,
Newport
Attn: B. E. Sandman, Code 213
Copy No. 14

Naval Undersea Warfare Center Division,
Newport
Attn: R. Philips, Code 8233
Copy No. 15

Naval Undersea Warfare Center Division,
Newport
Attn: D. McDowell, Bldg. 1302/2
Copy No. 16

Naval Undersea Warfare Center Division,
Newport
Attn: F. M. Cancilliere, Bldg. 990/5
Copy No. 17

Naval Undersea Warfare Center Division,
Newport
Attn: J. S. Hanson
Copy No. 18

~~Naval Undersea Warfare Center Division,~~
~~Newport~~
~~Attn: P. Madden~~
~~Copy No. 19~~

Naval Undersea Warfare Center Division,
Newport
Attn: S. Hassan, Bldg. 1302/2
Copy No. 20

Naval Undersea Warfare Center Division,
Newport
Attn: J. Muench, Bldg. 990/3
Copy No. 21

Naval Undersea Warfare Center Division,
Newport
Attn: T. Galib, Bldg. 106
Copy No. 22

Northrop Grumman Corporation
P.O. Box 1488
Annapolis, MD 21404
Attn: P. Madden
Copy No. 23

Northrop Grumman Corporation
Attn: R. W. Smith, MS 9105
Copy No. 24

Lockheed Martin Space Systems
3251 Hanover Street
palo Alto, CA 94304
Attn: P. D. Dean, Bldg. 203
Copy No. 25

Boston University
College of Engineering
110 Cummington Street
Boston, MA 02215
Attn: M. S. Howe
Copy No. 26

University of Chicago
5640 South Ellis Avenue
Chicago, IL 60637
Attn: L. P. Kadanoff, JFI Box 28, RI L-109
Copy No. 27

The Pennsylvania State University
The Applied Research Laboratory
P.O. Box 30
State College, PA 16804-0030
Attn: L. R. Hettche
Copy No. 28

ARL Penn State
Attn: R. Stern
Copy No. 29

ARL Penn State
Attn: G. C. Lauchle
Copy No. 30

ARL Penn State
Attn: M. L. Billet
Copy No. 31

ARL Penn State
Attn: C. H. Brickell
Copy No. 32

ARL Penn State
Attn: D. L. Bradley
Copy No. 33

ARL Penn State
Attn: Y.-Fan Hwang
Copy No. 34

ARL Penn State
Attn: H. J. Gibeling
Copy No. 35

ARL Penn State
Attn: R. C. Marboe
Copy No. 36

ARL Penn State
Attn: A. A. Atchley
Copy No. 37

ARL Penn State
Attn: S. Park
Copy No. 38

ARL Penn State
Attn: E. G. Liszka
Copy No. 39

ARL Penn State
Attn: D. E. Capone
Copy No. 40

ARL Penn State
Attn: T. A. Brungart
Copy No. 41

ARL Penn State
Attn: L. J. Peltier
Copy No. 42

ARL Penn State
Attn: S. Deutsch
Copy No. 37A

ARL Penn State
Attn: W. J. Hughes
Copy No. 38A

ARL Penn State
Attn: R. B. Cook
Copy No. 39A

ARL Penn State
Attn: S. A. Hambric
Copy No. 40A

ARL Penn State
Attn: D. C. Swanson
Copy No. 41A

ARL Penn State
Attn: ARL Library
Copy No. 42A

ARL Penn State
Attn: GTWT Library
Copy No. 43A

Added:

Director
Naval Research Laboratory
Washington, DC 20375
Copy No. 44

Defense Technical Documentation Center
8725 John J. Kingman Road
Suite 0944
Fort Belvoir, VA 22060
Copy Nos. 45 & 46

Office of Naval Research
5636 South Clark Street
Room 208
Chicago, IL 60605
Attn: David Wyner
Copy No. 47